Moqdad J. Dakhil
Department of Metallurgical, College of Materials Engineering, University of Babylon, Babylon, 51001
Iraq

Basem Al-Zubaidy
Department of Metallurgical, College of Materials Engineering, University of Babylon, Babylon, 51001
Iraq

Ruaa H. Kadhim
Department of Metallurgical, College of Materials Engineering, University of Babylon, Babylon, 51001
Iraq

Zainab Al-Khafaji
Department of Civil Engineering, Faculty of Engineering and Built Environment
Universiti Kebangsaan Malaysia, Bangi 43600
Malaysia
Department of Cooling and Air Conditioning Engineering, Imam Ja'afar Al-Sadiq University, Baghdad, 10001
Iraq

Effect of Selective Laser Melting Parameters on the Friction and Wear Performance of Ti-6Al-4V Alloy

Ti-6Al-4V has been widely used in the medical and dental fields due to its good biomechanical compatibility. Selective Laser Melting (SLM), an advanced metal powder-bed additive manufacturing method, offers versatility for tailoring part properties. However, further investigation is needed into the links between process parameters, volumetric energy density (VED), and resulting tribological performance. The present study focuses on the influence of varying VED levels on the porosity, surface finish, density , and wear behavior of Ti-6Al-4V. Five sets of samples were prepared at various VEDs. A higher VED results in densification, microhardness, and wear resistance, whereas a lower VED leads to increased porosity and roughness. The measured friction coefficient ranged from 0.266 to 0.63, and SEM observations identified smoother worn tracks in samples prepared under optimized conditions. These acid-etched results provide further, more direct evidence that VED must be closely controlled in SLM to enhance the durability and tribological properties of Ti–6Al–4V parts, thereby diminishing service life and expenditure in biomedical and industrial applications.

Keywords: *Additive manufacturing, Selective Laser Melting (SLM), Ti-6Al-4V, Wear Rate, Friction Coefficient.*

1. INTRODUCTION

Additive manufacturing (AM), often called three-dimensional printing, has evolved significantly since its inception in the 1980s, transforming from a quick-prototyping tool into a legitimate production technology for many applications [1]. AM is a layer-by-layer fabrication method characterized as "the process of joining materials to create a physical object from three-dimensional model data, commonly layer by layer, in contrast to subtractive manufacturing methods [2]. Metal AM encompasses a wide array of procedures utilizing various thermal energy sources and material deposition methods and is categorized by ASTM standards. The material is supplied to the system via a powder bed, wire-fed, or metal sheet system [3]. The metal is amalgamated using energy sources such as an electron beam or a laser beam. The mechanical and material qualities produced varied according to the energy sources and material dispersion procedures utilized [4]. The powder bed AM technique uses energy from a laser, known as Selective Laser Melting (SLM). SLM can produce intricate things without the need for further manufacturing post-processing [5,6]. The components produced by this technology were utilized across several sectors, including automotive, biomedical, aerospace, and tooling [7,8]. A wide variety of batch materials is available for SLM devices, with the most prevalent being commercial engineering materials, including steels, nickel-based superalloys, and titanium and their alloys [9]. SLM enables the fabrication of highly complex, precise, and lightweight structures, including porous or lattice implants that replicate bone mechanics and enhance tissue integration. Such implants can attain densities approaching 99%, providing superior strength and durability, while several studies [10,11] have demonstrated that additive manufacturing significantly reduces wear compared to conventional casting methods.

Nevertheless, investigations into the tribological behavior of Ti6Al4V as a friction pair remain limited [12,13]. The process parameters govern the microstructural development, mass density, and physical properties, including hardness and strength, of the end product in the SLM process [14]. Multiple factors in the SLM process affect the final product quality. Nevertheless, critical factors, including scanning speed, layer thickness, scan velocity, laser power, and hatch spacing, exert a more significant influence [15]. All factors, except for the scan pattern, generally converge to establish the volume energy density (VED), as delineated by Eq.(1), where P represents power in watts, V denotes scan velocity in milli-meters per second, h indicates scan distance in micro-meters, and d signifies the thickness of the deposited layer in micro-meters. The VED is expected to be articulated in J/mm³.

$$VED = \frac{P}{V * h * d} * 10^6 \quad (1)$$

Titanium (Ti) and its alloys, especially the widely used Ti-6Al-4V [16,17], have become high-performance materials for a wide range of applications in the aerospace, biomedical, and energy industries [13]. They

Received: Novembery 2025, Accepted: January 2026
Correspondence to: Dr. Zainab Al-Khafaji, Faculty of Engineering and Built Environment, University Kebangsaan Malaysia, Bangi, 43600, Malaysia
E-mail: P123005@siswa.ukm.edu.my
doi: 10.5937/fme2601107D

have been widely used due to their high corrosion resi–stance, high specific strength (the highest among metallic elements), low density , and good mechanical properties at high temperatures [18].

Unfortunately, despite these benefits, Ti-6Al-4V has several shortcomings in classical manufacturing. The alloy has a reputation for being hard to machine because its deformation behavior is complex, ranging from hot to cold, and, under extreme conditions, inclu–ding significant thermal softening at high temperatures, compared to metals such as steel or aluminum [19]. Furthermore, low thermal conductivity and lower volu–metric specific heat result in a higher cutting tempe–rature, which favours the formation of a build-up edge and increases tool wear [19,20].

Additive manufacturing (AM) processes have been widely investigated as an alternative route for fabrica–ting Ti-6Al-4V alloys to mitigate the drawbacks des–cribed. Selective Laser Melting (SLM) is one of them; it enables control over the part's geometry and micro–structure. In AM-processed Ti-6Al4V, rapid quenching and multiple heat cycling produce microstructures that differ from those of routinely processed materials. In particular, cooling rates of ~10^3–$10^{\square}$ K/s during SLM typically result in a refined martensitic α′ microstructure [21–23]. Although the fine microstructure contributes to high strength, it has the shortcomings of poor wear resistance and the release of Al and V ions, which may be harmful to long-term functioning in biomedical app–lications [24–29].

The tribological issues of Ti-6Al-4V alloys stem from titanium's inherent characteristics, particularly its poor tribological behaviour. These are high and unstable coefficients of friction (COF), low resistance to abrasive wear and adhesive wear, poor hardness, weak galling tendency, and limited load-carrying capacity [24], in this order, characterizing the most important tribological issues for the Ti-6Al-4V alloy.

While several studies investigated the effects of SLM processing parameters on various properties of Ti-6Al-4V, such as density, microstructure, and hardness, no combined research was found on mechanical and tribological performance during simultaneous variation of volumetric energy density (VED). This gap needs to be addressed to improve the alloy's performance, especially for bio-application s, as strength and wear resistance are critical. The goal of this work is to study the effect of SLM process parameters and, in particular, volumetric energy density (VED), on the physical, mechanical, and tribological properties of Ti-6Al-4V alloy. In particular, the studies aim to determine the influence of VED rates on % porosity, surface roughness, mass density, micro–hardness, and wear resistance.

2. MATERIALS AND METHODS

2.1 Powder Alloys

A Ti-6Al-4V powder is used to prepare the samples, and its chemical composition is shown in Table 1. The particle size distribution of the Ti6Al4V alloy powder, based on cumulative mass, is measured as follows: D10 = 20.88 µm, D50 = 39.90 µm, and D90 = 59.56 µm. Scanning electron microscopy (SEM) images of the powder grains, demonstrated in Figure 1, reveal that the particles are predominantly spherical or near-spherical with smooth surfaces.

2.2 Wear Test

Samples of solid cubic 8×8×8mm are prepared for this test. Before the test, the samples are ground with (180, 400, 1200, 2000) SiC papers. The samples are dried in an oven furnace at 90 degrees centigrade for 1 hour and cooled inside the furnace. An electric balance with ±0.0001 accuracy is utilized to weigh the samples. The samples are stored in silica gel to keep them completely dry. The pin-on-disk concept is used to study dry sliding wear, as shown in Figures 2(a) and (b). The tested specimen was mounted on the disk and brought into contact with a rotating steel pin at a sliding radius of 2.0 mm. The disc's rotation speed is fixed at 250 rpm, and the applied load is 5N. The sample is weighed after (15, 30, 45, 60, 75, and 90) minutes to determine the dry sliding wear rate according to equation (2). Figure 2 demonstrates the wear apparatus utilized in this work. The test method follows ASTM G 99-04 [30]. The wear rate is determined utilizing the formula (2):

Table 1. Chemical composition analysis of the Powder Ti-6Al-4V alloys

Element	Al	V	Fe	O	C	N	H	Y	Ti
Wet%	6.75	4.50	0.30	0.20	0.08	0.05	0.015	0.005	remainder

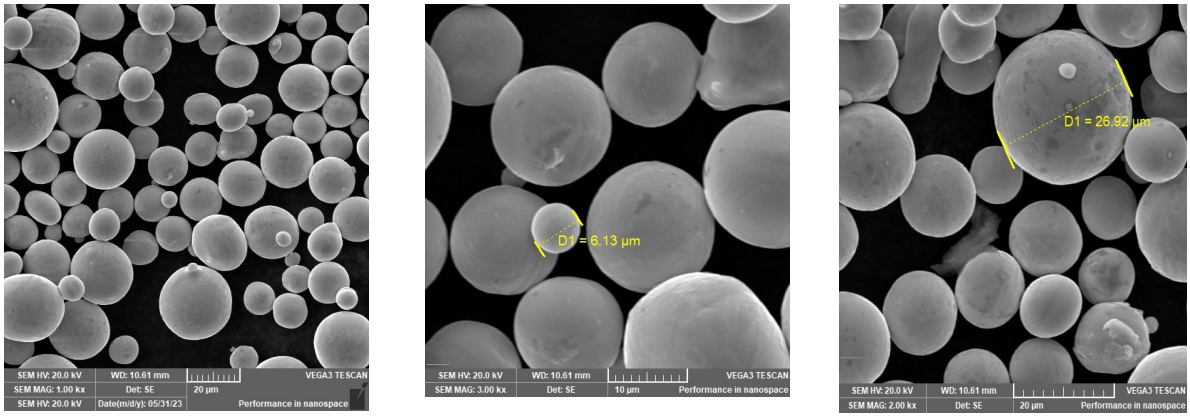

Figure 1. The morphology of Ti6Al4V powder.

$$Wear\ rate = \Delta W / \pi_{Rnt} \quad (2)$$

where: W = Weight loss (g) = Initial weight - Final weight,
R = Specimen radius to disc centre (m),
n = Rotational speed (*rpm*), and
t = Sliding time (minutes)

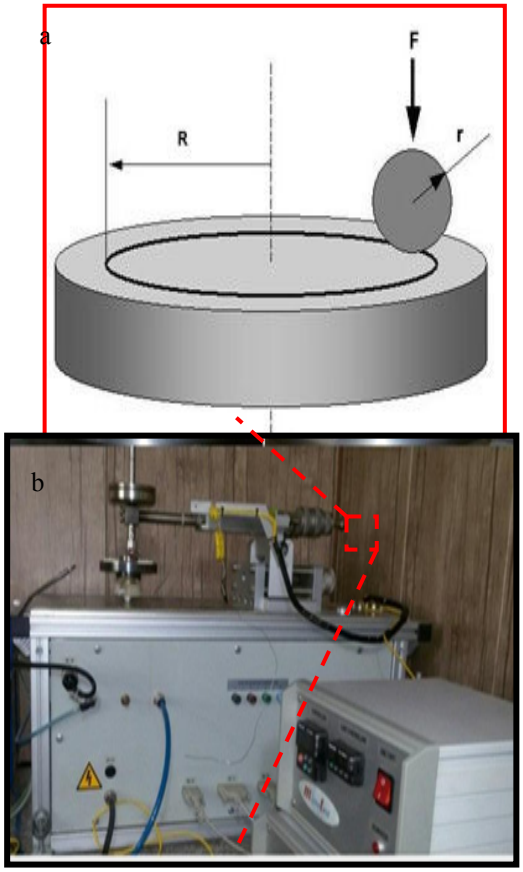

Figure 2. Schematic representation of the Pin-on-disc wear test machine of (a) the wear test machine, (b) the specimen configuration of the wear test.

2.3 Equipment

Porosity plays a crucial role in mechanical strength, wear, corrosion resistance, and tissue integration in biomedical applications, while density reflects material consolidation and overall structural integrity [31]. The porosity percentage is calculated utilizing Equation (3), where W1 is the actual weight, and *W2* is the theoretical weight. Each sample's mass density is determined by Archimedes' principle with ±0.0001 g accuracy (Ww) using formula (4). In this formula, *ρw*, *Wa*, and Ww denote the water mass density, the sample mass in air, and the sample mass in water, respectively. Phase analysis is performed using an XRD generator with a Cu target at a maximum tube voltage of 60 kV and a maximum tube current of 80 mA, with a 2θ scanning speed of 3°/min from 10° to 100°. Cu Kα radiation (λ = 1.5405 Å) is utilized for the XRD analysis. XRD analysis is performed utilizing the XRD-6000 Model, Shimadzu X-ray Diffract meter. Vickers micro hardness was measured using a digital micro-hardness tester (HVS-1000, Laryea), a load of **1.96 N** was applied with a dwell time of 15 s. Five indentations were performed on each specimen, and the average value was reported as the Vickers hardness (HV), the test procedure conformed to **ASTM E384**. The surface roughness of the specimens was assessed under different selective laser melting (SLM) process parameters using a TR210 surface roughness tester. For each parameter set, five measurements were taken, and the mean value was reported as the surface roughness.

The surface morphology of samples is evaluated utilizing a scanning electron microscope (SEM):

$$P\% = 1 - \frac{W_1}{W_2} * 100\% \quad (3)$$

$$\rho_m = \rho_W * \frac{W_a}{W_a - W_w} \quad (4)$$

2.4 Specimen Fabrication

As shown in Figure 3, the SLM method is used to create cubic samples (8 × 8 × 8 mm), using many sets of process variables listed in Table 2. Every sample has a layer thickness of 30 µm. The environment used for sample manufacturing is argon. A Metal three-dimen–sional printer (NOURA Company type M1OOP) with a 300 W fibre laser, 80 µm spot size, and a construction volume of Ø=125×h=150 mm is used in the SLM process. The locations of the construction and powder platforms, the number of layers completed and yet to be completed, the time remaining, and other pertinent information are all included in the comprehensive infor–mation on the construction procedure provided by the NOURA SLM program. The checkerboard scan tech–nique, which divides the print area into smaller square portions and scans them sequentially, was used in this study. In SLM-produced Ti-6Al-4V components, this technique is well known for striking a balance between mechanical integrity, temperature control, and dimensional precision [34]. As seen in Figure 4, the scanning direction is rotated between subsequent layers. An estimated measurement error of ±2.083% was used to assess SLM-fabricated Ti-6Al-4V specimens, accounting for variations in process variability and equipment accuracy.

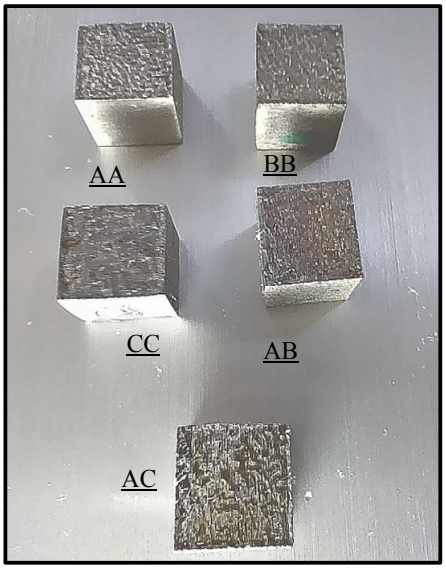

Figure 3. As-built Ti-6Al-4V specimens were fabricated under various SLM parameter settings.

VED, as in Table 2, which integrates laser power, scanning speed, hatch spacing, and layer thickness, was selected to optimize powder melting and part consolida–tion in SLM. The chosen VED values prevent insuffici–ent melting (causing porosity and weak strength) and av–oid excessive energy input (leading to keyholing, elem–ent evaporation, and residual stresses). Based on litera–ture and preliminary experiments, the applied VED range ensures high-density, defect-minimized Ti-6Al-4V com–ponents with reliable mechanical performance [35–37].

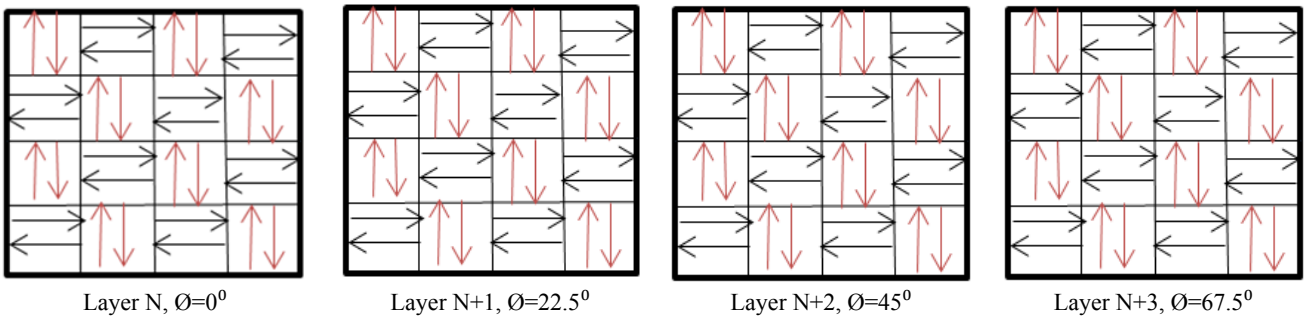

Figure 4. The scan strategy uses a checkerboard pattern.

Table 2. Parameters of the SLM process applied for specimen fabrication.

Specimen	P (W)	h (μm)	v (mm/s)	VED (J/mm3)	Scan pattern
AA	240	0.09	1000	88.88888889	Chessboard(2*2mm)
BB	160	0.09	1250	47.407	
CC	160	0.12	1500	29.62962963	
AB	200	0.09	1500	49.38271605	
AC	200	0.12	1000	55.55555556	

3. RESULTS AND DISCUSSIONS

3.1 Microstructural Analysis (XRD)

Figure 5 demonstrates the X-ray diffraction (XRD) pat–terns of cubic Ti-6Al-4V samples manufactured utili–zing SLM under different processing conditions. For the AA sample, distinct diffraction peaks were observed at 2θ values of 35.08°, 38.39°, 40.16°, 52.98°, 62.94°, and 75.95°, corresponding to the α′ martensitic phase, with reflections from the (100), (002), (101), (102), (103), and (110) planes. These results confirm that the AA sample exhibits a fully martensitic microstructure, attri–buted to the high-volume-energy-density (VED) applied during SLM. The high VED promotes complete melting followed by rapid cooling, which enhances the forma–tion and maintenance of the stable α′ phase. These re–sults are consistent with previous studies [37]. In con–trast, samples BB, AB, and AC, which were made with lower VED values, demonstrate the retention of a por–tion of the β-Ti phase because of slower cooling rates that allow the retention of the β phase. In the case of sample CC, the XRD pattern shows weak, broad peaks, indicating poor crystallinity and the possible presence of the β phase due to insufficient energy input, leading to incomplete melting, high porosity, and low mass den–sity. Characteristic diffraction peaks of the β phase are observed at 2θ values of 38.39°, 52.98°, 69.94°, and 82.29°, corresponding to the β (110), β (200), β (211), and β (220) planes, respectively.

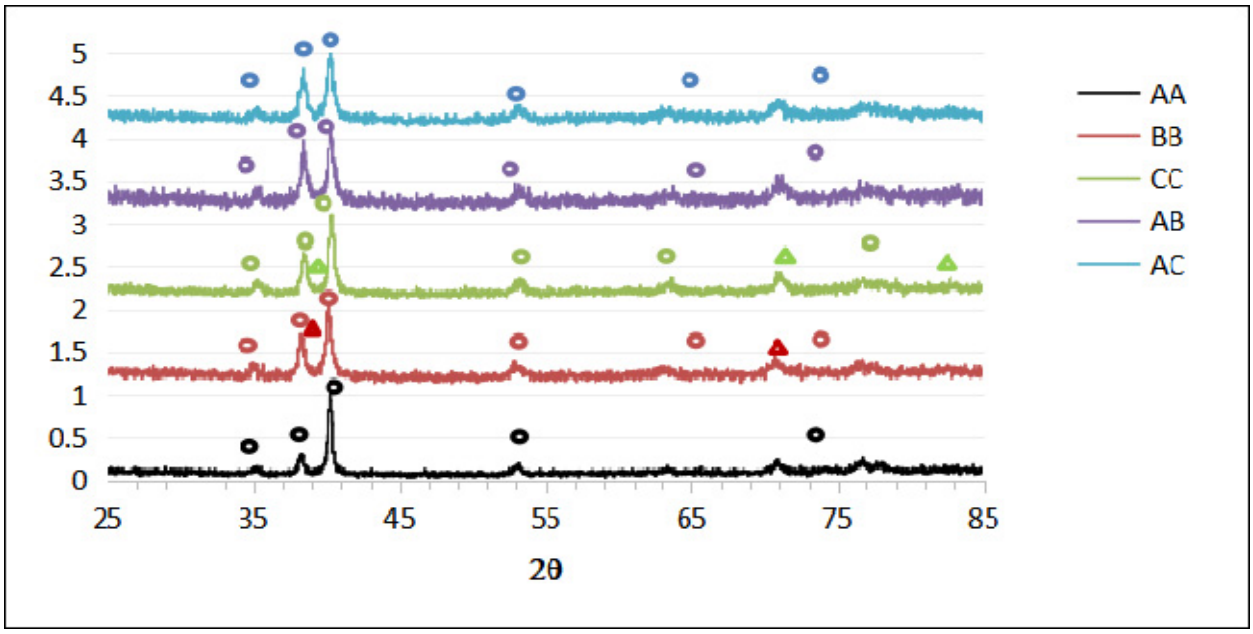

Figure 5. The X-ray diffraction (XRD) patterns of cubic Ti-6Al-4V samples.

3.2 Physical Properties (Density, Porosity, Ra)

However, it should be noted that the porosities present in the final part are a consequence of incomplete mel–ting if the volumetric energy density is not sufficient to melt and disperse the powder. Furthermore, increasing the scan–ning speed and hatch spacing (or reducing the laser power) may increase the surface roughness of SLM-produced Ti6Al4V components. The effects of VED on mass density, porosity, and surface roughness (Ra) are presented in Figures 6 and 7. There is a clear relationship between the applied VED and the subse–quent structural integrity and surface characteristics of printed samples. The sample CC prepared with the lowest VED (29.629 J/mm³) had the highest porosity (6.478%) and surface roughness Ra (3.479 µm), indicating insufficient mel–ting and bonding between powder layers, resulting in very low densification and a rough, porous surface.

Additionally, pores condense on the surface when sufficient input energy is applied, thereby increasing the surface tension and capillary pressure at the solid-liquid interface, resulting in smaller SLM samples. A lower scan–ning speed ensures continuous scanning along a trajec–tory. The small pitch of the hatch would increase the overlap between adjacent scan lines, so that a powder in the vertical direction would be fully fused between them.

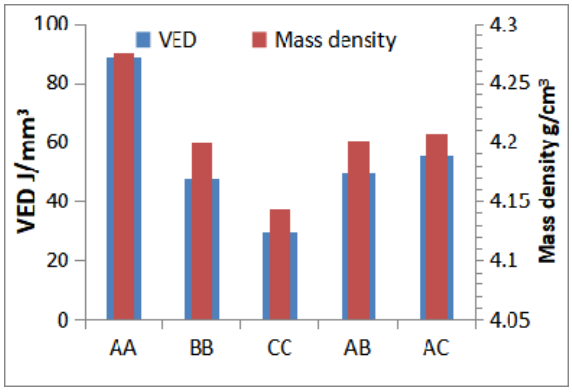

Figure 6. Relationships between the samples' mass density and VED.

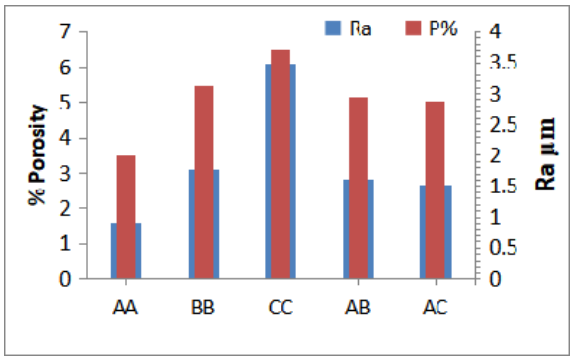

Figure 7. Relationships between the Porosity% and Surface roughness of the specimens.

However, the CC sample with the first VED achi–eved showed lower density (4.143 g/cm³), proving that excessive energy is harmful to its performance. Shift became more pronounced in sample AA (88.88 J/mm³), which had a relatively lower porosity of 3.477% and a smoother surface Ra (0.913 µm). This enhancement is suggested to stem from improved laser-material inter–action, resulting in a more homogeneous melt and redu–ced void formation. In addition, these mass density re–sults are consistent with the VED tendency. Specimens AA achieved the highest densities (4.276 g/cm³), which indicated nearly full densification and the minimum level of internal porosity, improved energy density due to which an increase in melt pool wettability as well as a reduction in the difference of surface tension, and a decrease in balling can be expected; hence, low level of surface roughness was assured [38].

3.3 Mechanical Properties (Hardness)

The VED is a critical factor in SLM, directly proporti–onal to the laser power and inversely proportional to both the scan speed and hatch spacing, as expressed in Equation (1). Based on the data presented in Table 2 and Figures 6 and 7, a clear relationship between VED and porosity is observed. Notably, insufficient energy input prevents complete dissolution and merging of powder particles, leading to incomplete melting and the formation of pores. An increase in scan speed or hatch spacing, or a reduction in laser power, leads to a decrease in melt pool volume. This reduces the extent of powder consolidation, leaving voids trapped among partially melted particles beneath the solidified hatch lines. Consequently, porosity increases, thereby lowering the overall density and structural integrity of the fabricated part.

Furthermore, the microhardness profiles (Figure 8) of the Ti-6Al-4V samples fabricated via SLM demon–strated a strong correlation with the applied VED. Spe–cimen AA, processed with the highest VED of 88.88 J/mm³, exhibited the highest microhardness, exceeding 1050 HV. This enhancement in hardness is attributed to rapid solidification conditions that promoted the forma–tion of the martensitic α′ phase, along with reduced surface porosity and a low roughness value. Conversely, specimen CC, fabricated at the lowest VED of 29.63 J/mm³, recorded significantly lower microhardness va–lues since insufficient dissolution results in increased porosity and a higher percentage of retained β phase.

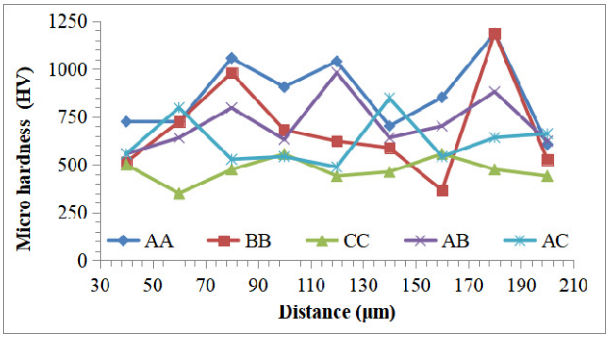

Figure 8. The micro hardness profiles of cubic Ti-6Al-4V samples.

3.4 Tribological Behavior (Friction, Wear)

3.4.1 Coefficient of Friction Behaviour

The average friction coefficient of the Ti-6Al-4V samp–les fabricated by SLM was evaluated under different

conditions, as measured during a dry-sliding wear test. The values of the friction coefficient were around 0.266 to 0.63, and there were values of the friction coefficient of the sample (BB, AB, and AC) that ranged between these two values. The evolution of the coefficient of friction over time during wear tests of samples under different SLM conditions (Table 2) is shown in Figure 9. The elevated coefficient of friction observed for the CC sample (0.63), in contrast to the lower value for the AA sample (0.266), can be attributed to variations in the SLM processing factors, particularly the volume energy density (VED). The CC sample was fabricated utilizing a lower VED, which likely led to increased surface roughness, higher porosity, and the formation of an unstable oxide layer due to incomplete powder fusion. These factors collectively contributed to higher friction during sliding.

In contrast, the AA sample, processed with a higher VED, exhibited improved surface integrity and oxide stability, resulting in a significantly lower coefficient of friction. All samples under different factors reach a steady-state friction coefficient within a few seconds of the test due to the rapid formation of the passive surface layer and the intrinsic tribological stability of Ti64 alloy under static testing conditions [39]. In SLM-produced Ti-6Al-4V samples, the coefficient of friction initially increases during a run-in period, associated with mec–hanical removal of the native passive TiO□ layer (depas–sivation) and exposure of the active titanium surface to the counterbody (ball), temporarily increasing friction. However, since the rapid re-passivation and the alloy's inherent tribological properties, a steady-state friction coefficient is reached within a few seconds of testing.

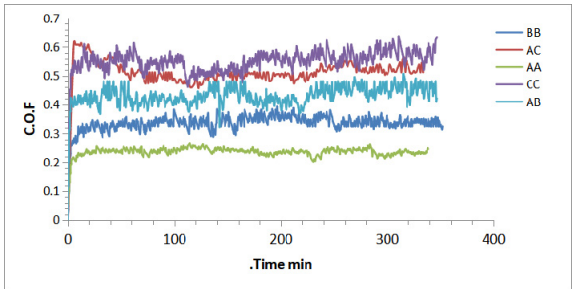

Figure 9. Friction coefficient against duration plot for different surfaces at the pin-on-disk wear test.

3.4.2 Wear Rate Behavior

As demonstrated in Figure 10, the variation of wear rate (g/mm³) as a function of sliding time (min) for five various specimens (AA, BB, CC, AB, AC). An apparent variation in wear rate was observed among the SLM-fabricated Ti-6Al-4V samples, directly influenced by the applied volume energy density (VED). Sample AA, processed with the highest VED (88.89 J/mm³), exhibited superior wear resistance with the lowest wear rate (0.000018 g/mm³), owing to complete powder melting and the formation of a dense, low-porosity microstruc–ture. In contrast, sample CC, fabricated under the lowest VED (29.63 J/mm³) and the highest scan speed (1500 mm/s), demonstrated the highest wear rate (0.000032 g/mm³), primarily due to insufficient energy input, poor interlayer bonding, and increased porosity. Intermediate behavior was noted in samples BB, AB, and AC. Among them, sample AC demonstrated improved wear perfor–mance, likely due to a more balanced VED (55.56 J/mm³) and a reduced scan speed, which enhanced heat input and densification. Overall, the results confirm an inverse rela–tionship between wear rate and microhardness, reinfor–cing the well-established principle that higher surface hardness correlates with better tribological performance.

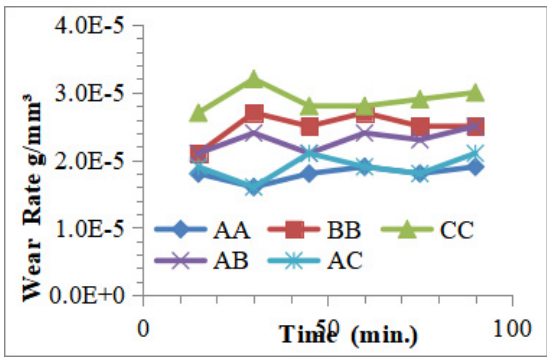

Figure 10. The variation of wear rate (g/mm³) as a function of sliding time (min) for five various specimens.

3.5 SEM Characterization

The SEM micrographs presented illustrate the morp–hological characteristics of the wear tracks on Ti-6Al-4V alloy specimens fabricated via SLM and subjected to dry sliding wear under varying operational conditions. The surface morphology reveals a diverse range of wear mechanisms, including abrasive, adhesive, oxidative, and third-body wear, reflecting the complex tribological response of SLM-processed Ti-6Al-4V alloys. Speci–mens such as AA and AB exhibit parallel grooves with minor surface damage, indicating dominant abra–sive wear with minimal plastic deformation under rela–tively mild conditions. In contrast, samples BB and CC exhibit more severe wear, characterized by deep ploughing grooves, plastic smearing, and rhomboidal strain pat–terns, indicating the onset of adhesive wear and loca–lized material softening due to elevated frictional hea–ting. The magnified CC region further reveals extensive plastic deformation and possible surface flow, sugges–ting intense interfacial shear. Moreover, the presence of voids, fragmented oxides, and embedded debris, particularly in samples AC and AB (zoomed), indicates the synergistic action of oxidative and third-body abrasion, exacerbated by residual porosity and unmelted particles, which are commonly associated with SLM-induced microstructural heterogeneity [40,41].

Table (3) provides a consolidated overview of the experimental results and confirms the decisive role of volumetric energy density (VED) in governing the quality of additively manufactured specimens. Incre–asing VED resulted in a marked reduction in porosity (from 6.48 ± 0.09% to 3.49 ± 0.04%) and surface roughness (from 3.48 ± 0.12 µm to 0.91 ± 0.05 µm), accompanied by a slight improvement in density (from 4.143 ± 0.03 to 4.276 ± 0.01 g/cm³). These micro–structural improvements were reflected in better tribo–logical performance, with the COF and wear track width values decreasing (0.67 ± 0.04 to 0.26 ± 0.02; and 1985 ± 22 µ µm to 1420 ± 15 µm, respectively).

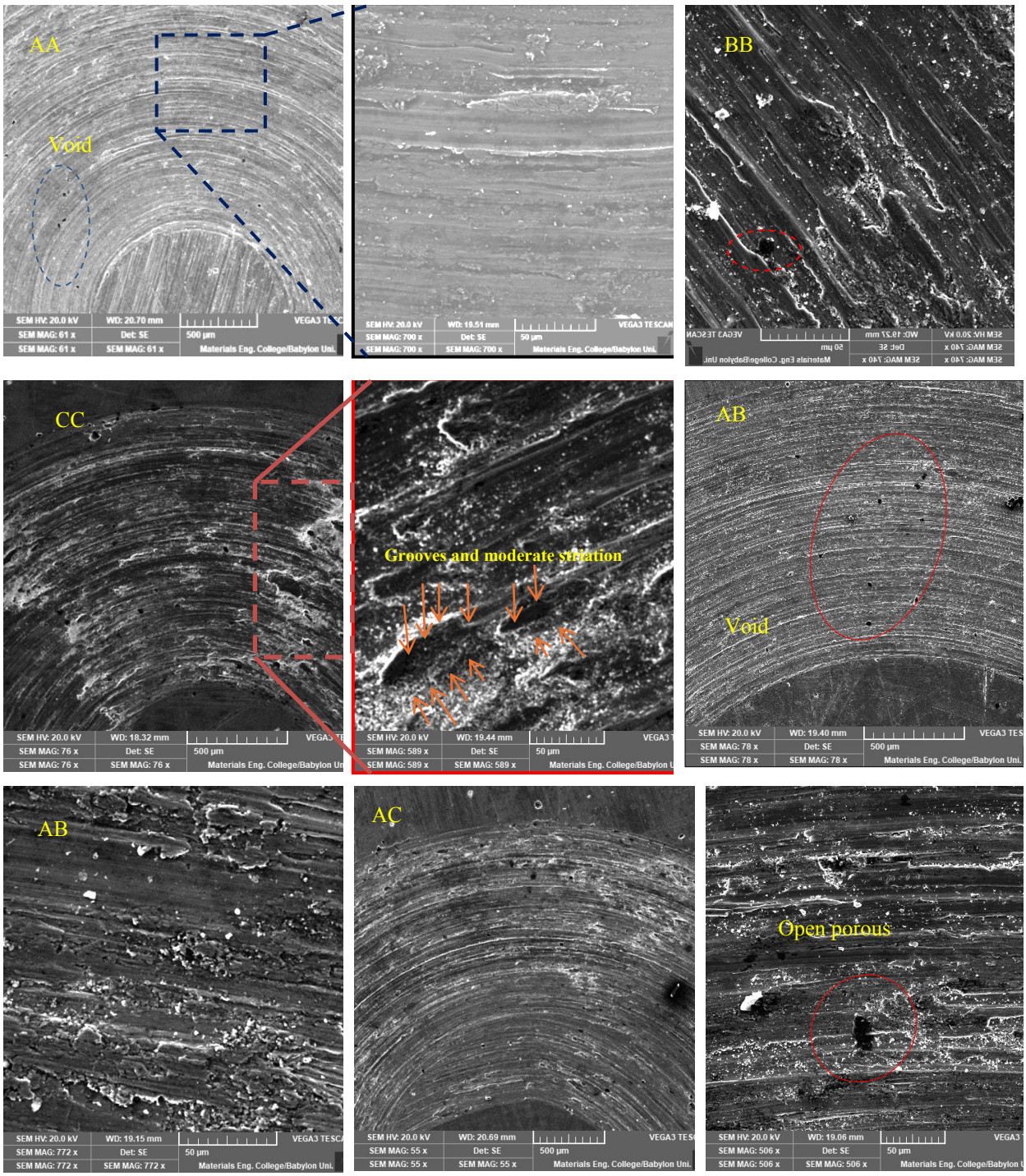

Figure 11. SEM micrographs of the wear track on Ti-6Al-4V samples fabricated by SLM under different conditions, showing grooves, voids, and delamination features formed during the wear process.

Table 3. Summary of the effects of volumetric energy density (VED) on porosity, surface roughness, mass density, coefficient of friction, and wear track width of SLM-fabricated Ti-6Al-4V samples.

Specimen	VED (J/mm³)	Porosity (%)	Ra (μm)	Density g/cm³)	C.O.F	Wear track width (μm)
AA	88.88888889	3.49 ± 0.04	0.91 ± 0.05	4.276 ± 0.01	0.26 ± 0.02	1420 ± 15
BB	47.407	5.48 ± 0.07	1.77 ± 0.08	4.20 ± 0.02	0.36 ± 0.03	1493 ± 18
CC	29.62962963	6.48 ± 0.09	3.48 ± 0.12	4.143 ± 0.03	0.67 ± 0.04	1985 ± 22
AB	49.38271605	5.15 ± 0.06	1.62 ± 0.07	4.202 ± 0.02	0.47 ± 0.03	1588 ± 19
AC	55.55555556	5.03 ± 0.05	1.53 ± 0.06	4.207 ± 0.02	0.50 ± 0.03	1607 ± 20

The standard deviations have been included to highlight the repeatability of the measurements and underpin the credibility of trends. Overall, the results indicate that an appropriately high VED promotes densification, smooth surface formation, and enhanced wear resistance, whereas an insufficient VED leads to defects, higher friction, and accelerated wear. Because VED is controlled by the interplay among laser power, scan

speed, and hatch spacing, fine-tuning these processing parameters is important to optimize both microstructural integrity and end-use performance.

4. CONCLUSION

The present work indicates that the VED is the critical parameter governing microstructure and tribology of SLM-processed Ti-6Al-4V components. By increasing the VED from 29.6 to 88.9 J/mm³, a 46% decrease in porosity and a 74% decrease in surface roughness were achieved , with a roughly 3% increase in density. The enhanced tribological response was characterized by a reduction in the coefficient of friction (61%) and the wear track width (by ~29%), which were associated with a dense, defect-poor microstructure and a smoother surface morphology that diminishes direct metal-to-metal contact. The above results indicate that by properly adjusting SLM parameters, it is possible to produce Ti-6Al-4V parts with better surface integrity and wear resistance, which are important for biomaterial applications. However, the study is confined to laboratory tribological testing and does not account for fatigue, corrosion, or long- term performance. Further studies are necessary to investigate these aspects, explore post-processing effects, and conduct multi-response optimization, thereby enabling a more thorough understanding of the relationships among microstructure, stroke processing, and tribological performance.

REFERENCES

[1] Zhou L, Miller J, Vezza J, Mayster M, Raffay M, Justice Q, et al. Additive Manufacturing: A Comprehensive Review. Sensors 2024;24:2668. https://doi.org/10.3390/s24092668.

[2] Bănică C-F, Sover A, Anghel D-C. Printing the Future Layer by Layer: A Comprehensive Exploration of Additive Manufacturing in the Era of Industry 4.0. Appl Sci 2024;14:9919. https://doi.org/10.3390/app14219919.

[3] Srivastava M, Rathee S, Patel V, Kumar A, Koppad PG. A review of various materials for additive manufacturing: Recent trends and processing issues. J Mater Res Technol 2022;21:2612–41. https://doi.org/10.1016/j.jmrt.2022.10.015.

[4] Taghian M, Mosallanejad MH, Lannunziata E, Del Greco G, Iuliano L, Saboori A. Laser powder bed fusion of metallic components: Latest progress in productivity, quality, and cost perspectives. J Mater Res Technol 2023;27:6484–500. https://doi.org/10.1016/j.jmrt.2023.11.049.

[5] Narasimharaju SR, Zeng W, See TL, Zhu Z, Scott P, Jiang X, et al. A comprehensive review on laser powder bed fusion of steels: Processing, micro–structure, defects and control methods, mechanical properties, current challenges and future trends. J Manuf Process 2022;75:375–414. https://doi.org/10.1016/j.jmapro.2021.12.033.

[6] Kumar B, Aravindan KM, Jebaraj AV, Kumar TS. Effect of Post-Fabrication Treatments on Surface Residual Stresses of Additive Manufactured Stainless Steel 316L. FME Trans 2021;49.

[7] Singh N, Hameed P, Ummethala R, Manivasagam G, Prashanth KG, Eckert J. Selective laser manu–facturing of Ti-based alloys and composites: impact of process parameters, application trends, and future prospects. Mater Today Adv 2020; 8:100097. https://doi.org/10.1016/j.mtadv.2020.100097.

[8] Wang H, Klaric S, Havrlišan S. Preliminary study of bead-on-plate welding bead geometry for 316L stainless steel using GMAW. FME Trans 2024;52:563–72.

[9] Khanna N, Zadafiya K, Patel T, Kaynak Y, Rahman Rashid RA, Vafadar A. Review on machining of additively manufactured nickel and titanium alloys. J Mater Res Technol 2021;15:3192–221. https://doi.org/10.1016/j.jmrt.2021.09.088.

[10] Bartolomeu F, Buciumeanu M, Pinto E, Alves N, Silva FS, Carvalho O, et al. Wear behavior of Ti6Al4V biomedical alloys processed by selective laser melting, hot pressing, and conventional cas–ting. Trans Nonferrous Met Soc China 2017; 27:829–38. https://doi.org/10.1016/s1003-6326(17)60060-8.

[11] Goyal V, Verma G. Tribological Behavior of Direct Metal Laser Sintering–Manufactured Ti6Al4V Al–loy in Different Biofluids for Orthopedic Implants. J Tribol 2024;146. https://doi.org/10.1115/1.4064506.

[12] Dixit S et al. Effect of solutionizing temperature and cooling rate on phase morphology, recrysta–llization and texture evolution in a heat treated Ti□6Al□4Valloy having different types of micro–structure. J Alloys Compd 2022;927:166897. https://doi.org/10.1016/j.jallcom.2022.166897.

[13] Jasim Ahmed Jasim;, Yaser A, Al-Khafaji Z. An ANSYS simulation study on the effect of applying tita-nium alloy (Ti-6Al-4V) coating for wind turbine gear. Acad J Manuf Eng 2024;22.

[14] Saedi S, Shayesteh Moghaddam N, Amerinatanzi A, Elahinia M, Karaca HE. On the effects of selective laser melting process parameters on microstructure and thermomechanical response of Ni-rich NiTi. Acta Mater 2018;144:552–60. https://doi.org/10.1016/j.actamat.2017.10.072.

[15] Simonelli M. et al. A Study on the Laser Spatter and the Oxidation Reactions During Selective Laser Melting of 316L Stainless Steel, Al-Si10-Mg, and Ti-6Al-4V. Metall Mater Trans A 2015;46:3842–51. https://doi.org/10.1007/s11661-015-2882-8.

[16] Al-Zubaidy B, Radhi NS, Al-Khafaji ZS. Study the effect of thermal impact on the modelling of (titanium-titania) functionally graded materials by using finite element analysis. Int J Mech Eng Technol 2019.

[17] Srećković M, Milosavljević A, Kovačević A, Gospavić R, Trtica M, Ristić Z, et al. Interaction of lasers of various types with alloys based on Ni and Ti. FME Trans 2008;36:167–73.

[18] Yang L, Ramachandran S, Bagasol A, Guan Q, Wang W, Browne DJ, et al. Solidification micro–structure variations in additively manufactured Ti-6Al-4V using laser powder bed fusion. Scr Mater 2023;231:115430. https://doi.org/10.1016/j.scriptamat.2023.115430.

[19] Motyka M. Martensite Formation and Decom–position during Traditional and AM Processing of Two-Phase Titanium Alloys—An Overview. Metals (Basel) 2021;11:481. https://doi.org/10.3390/met11030481.

[20] Yang Z, Li Y, Wei X, Wang X, Wang C. Marten–site Start Temperature Prediction through a Deep Learning Strategy Using Both Microstructure Ima–ges and Composition Data. Materials (Basel) 2023; 16:932. https://doi.org/10.3390/ma16030932.

[21] de Formanoir C, Martin G, Prima F, Allain SYP, Dessolier T, Sun F, et al. Micromechanical beha–vior and thermal stability of a dual-phase α+α' titanium alloy produced by additive manufacturing. Acta Mater 2019;162:149–62. https://doi.org/10.1016/j.actamat.2018.09.050.

[22] Tan C, Zhou K, Kuang M, Ma W, Kuang T. Micro–structural characterization and properties of selec–tive laser melted maraging steel with different build directions. Sci Technol Adv Mater 2018;19:746–58. https://doi.org/10.1080/14686996.2018.1527645.

[23] Brunette DM, Tengvall P, Textor M, Thomsen P. Titanium in medicine: material science, surface sci–ence, engineering, biological responses and medical applications. Springer; 2001.

[24] Leyens C, Peters M. Titanium and titanium alloys: fundamentals and applications. Wiley Online Lib–rary; 2006.

[25] Pramanik A. Problems and solutions in machining of titanium alloys. Int J Adv Manuf Technol 2013; 70: 919–28. https://doi.org/10.1007/s00170-013-5326-x.

[26] Parry L, Ashcroft IA, Wildman RD. Understanding the effect of laser scan strategy on residual stress in selective laser melting through thermo-mechanical simulation. Addit Manuf 2016;12:1–15. https://doi.org/10.1016/j.addma.2016.05.014.

[27] [27] Win Khun N, Quan Toh W, Liu E. Study on Changes in Hardness and Wear Resistance of 3D Printed Ti6Al4V with Heat Treatment Temperature. Tribol Ind 2023;45:129–35. https://doi.org/ 10.24874/ti.1421.12.22.02.

[28] Haase F et al. Aluminum- and Vanadium-free Titanium Alloys for Medical Applications. MATEC Web Conf 2020;321:5008. https://doi.org/10.1051/matecconf/202032105008.

[29] Łępicka M, Grądzka-Dahlke M. Surface modifi–cation of Ti6Al4V titanium alloy for biomedical applications and its effect on tribological performance-a review. Rev Adv Mater Sci 2016;46.

[30] Houdkova S, Kasparova M, Zahalka S, Vyzkum F. The friction properties of the HVOF sprayed coatings suitable for combustion engines, measured in compliance with ASTM G-99. WIT Trans Eng Sci 2010;66:129–39.

[31] Fojt J, Joska L, Málek J. Corrosion behaviour of porous Ti–39Nb alloy for biomedical applications. Corros Sci 2013;71:78–83. https://doi.org/10.1016/j.corsci.2013.03.007.

[32] Yu G, et al. The select of internal architecture for porous Ti alloy scaffold: A compromise between mechanical properties and permeability. Mater & Des 2020;192:108754. https://doi.org/10.1016/j.matdes.2020.108754.

[33] ASTM A. B962-17-Standard Test Methods for Density of Compacted or Sintered Powder Metal–lurgy (PM) Products Using Archimedes' Principle. Am Soc Test Mater West Conshohocken, PA, USA 2017.

[34] Wei W-H, Shen J. Effect of laser energy density on microstructures and mechanical properties of selec–tive laser melted Ti-6Al-4V alloy. Int J Mater Res 2018;109:437–42. https://doi.org/10.3139/146.111615.

[35] Wu G, Wu H, Zhang X, Xiao S, Wu Z, Chu PK. Electrochemical degradation and extraction capabi–lity of magnesium wastes in sewage treatment. Mater Des 2016;111:537–40.

[36] Mugwagwa L, Dimitrov D, Matope S, Yadroitsev I. Evaluation of the impact of scanning strategies on residual stresses in selective laser melting. Int J Adv Manuf Technol 2019;102:2441–50. https://doi.org/10.1007/s00170-019-03396-9.

[37] Javidrad HR, Ghanbari M, Javidrad F. Effect of scanning pattern and volumetric energy density on the properties of selective laser melting Ti-6Al-4V specimens. J Mater Res Technol 2021;12:989–98. https://doi.org/10.1016/j.jmrt.2021.03.044.

[38] Chlebus E, Kuźnicka B, Kurzynowski T, Dybała B. Microstructure and mechanical behaviour of Ti-6Al-7Nb alloy produced by selective laser melting. Mater Charact 2011;62:488–95. https://doi.org/10.1016/j.matchar.2011.03.006.

[39] Mace AO, Kurtz MA, Gilbert JL. Fretting and Fretting Corrosion Behavior of Additively Manu–factured Ti-6Al-4V and Ti-Nb-Zr Alloys in Air and Physiological Solutions. J Funct Biomater 2024; 15:38. https://doi.org/10.3390/jfb15020038.

[40] Rajeev C et al. Impact of Laser Shock Peening on Corrosion Performance of Selective Laser Melted Stainless Steel 316L. Surfaces and Interfaces 2026: 108412.

[41] Dakhil MJ, AbidAli AK, Al-Khafaji Z. Optimiza–tion of selective laser melting parameters of Ti6Al4V alloys lattice structures utilizing taguchi method and grey relational analysis. Biomed Eng Commun 2026;5:16.

УТИЦАЈ ПАРАМЕТАРА СЕЛЕКТИВНОГ ЛАСЕРСКОГ ТОПЉЕЊА НА ПЕРФОРМАНСЕ ТРЕЊА И ХАБАЊА ЛЕГУРЕ TI-6AL-4V

М.Ц. Дакил, Б. Ал-Зубаиди, Р.Х. Кадим, З. Ал-Кафађи

Ti-6Al-4V се широко користи у медицинској и стоматолошкој области због своје добре биомеханичке компатибилности. Селективно ласерско топљење (SLM), напредна метода адитивне производње у слоју металног праха, нуди свестраност за прилагођавање својстава делова. Међутим, потребна су даља истраживања веза између параметара процеса, запреминске густине енергије (VED) и резултирајућих триболошких перформанси. Ова студија се фокусира на утицај различитих нивоа VED на порозност, завршну обраду површине, густину и понашање хабања Ti-6Al-4V. Пет комплета узорака је припремљено при различитим VED-овима. Већи VED резултира згушњавањем, микротврдоћом и отпорношћу на хабање, док нижи VED доводи до повећане порозности и храпавости. Измерени коефицијент трења кретао се од 0,266 до 0,63, а SEM посматрања су идентификовала глатке трагове хабања у узорцима припремљеним под оптимизованим условима. Ови резултати нагризања киселином пружају додатне, директније доказе да се VED мора пажљиво контролисати у SLM-у како би се побољшала издржљивост и триболошка својства Ti–6Al–4V делова, чиме се смањује век трајања и трошкови у биомедицинским и индустријским применама.